10-22-2004

Melting points and thermal expansivities of proton-disordered hexagonal ice with several model potentials

Yuji Koyama
Okayama University

Hideki Tanaka
Okayama University, htanakaa@cc.okayama-u.ac.jp

Guangtu Gao
University of Nebraska - Lincoln

Xiao Cheng Zeng
University of Nebraska-Lincoln, xzeng1@unl.edu

Melting points and thermal expansivities of proton-disordered hexagonal ice with several model potentials

Yuji Koyama and Hideki Tanaka[a)]
Department of Chemistry, Faculty of Science, Okayama University, 3-1-1 Tsushima, Okayama 700-8530, Japan

Guangtu Gao and X. C. Zeng
Department of Chemistry and Center for Materials Research & Analysis, University of Nebraska, Lincoln, Nebraska 68588

(Received 25 June 2004; accepted 6 August 2004)

A method of free energy calculation is proposed, which enables to cover a wide range of pressure and temperature. The free energies of proton-disordered hexagonal ice (ice Ih) and liquid water are calculated for the TIP4P [J. Chem. Phys. **79**, 926 (1983)] model and the TIP5P [J. Chem. Phys. **112**, 8910 (2000)] model. From the calculated free energy curves, we determine the melting point of the proton-disordered hexagonal ice at 0.1 MPa (atmospheric pressure), 50 MPa, 100 MPa, and 200 MPa. The melting temperatures at atmospheric pressure for the TIP4P ice and the TIP5P ice are found to be about $T_m = 229$ K and $T_m = 268$ K, respectively. The melting temperatures decrease as the pressure is increased, a feature consistent with the pressure dependence of the melting point for realistic proton-disordered hexagonal ice. We also calculate the thermal expansivity of the model ices. Negative thermal expansivity is observed at the low temperature region for the TIP4P ice, but not for the TIP5P ice at the ambient pressure. © *2004 American Institute of Physics.*
[DOI: 10.1063/1.1801272]

I. INTRODUCTION

Simple rigid models of water have been proven to be very useful in studying physical properties of liquid water by computer simulation. Various models for water dimer have been developed. Among them, the simple point charge model such as SPC (Ref. 1) or SPC/E,[2] and the transferable intermolecular potential model such as TIP3P (Ref. 3) or TIP4P (Ref. 4) have been widely used today either for the study of pure water or aqueous solutions. These models can reproduce many properties of water successfully. One well-known physical property of liquid water is the peculiar dependence of its density on temperature. For example, liquid water at atmospheric pressure exhibits a temperature of maximum density (TMD) at 277 K. Many attempts have been made to reproduce the TMD via computer simulation.[5–7] Some water models can yield the density maximum,[6–11] but the maximum appears at temperature region far from the experimental result. Thus far, no model can quantitatively reproduce the TMD except the TIP5P model proposed by Mahoney and Jorgensen.[12] The TIP5P model does yield a density maximum near 277 K, which corresponds to realistic water very well.[12]

In this work, we carried out two different calculations to examine the extent to which the TIP5P model can reproduce some other anomalous properties of water and ice. First, we calculate the melting point of the proton-disordered hexagonal TIP5P ice over wide temperature-pressure range. As a comparison, the melting point of the TIP4P model is also calculated. It is important to know the exact location of the melting point of ice Ih, especially when theoretical prediction of formation and dissociation of clathrates as well as various properties of the water in the supercooling region are considered. Second, we calculate the thermal expansivity of the TIP5P ice. It is well known that the thermal expansivity of ice Ih is negative below temperature 60 K,[13] arising from anomalous negative Grüneisen parameters. Thus, the negative thermal expansivity can be a stringent test of water model since the negative thermal expansivity is typical of the tetrahedrally coordinated substance. The negative thermal expansivity was successfully reproduced by computer simulation using the TIP4P potential function.[14]

II. MODEL AND METHOD

A. The TIP4P and TIP5P potential functions and generation of ice Ih structure

In both the TIP4P and the TIP5P models, the OH bond length and HOH bond angle are set to the experimental gas-phase value, i.e., 0.9572 Å and 104.52 Å. Both models have two positive point charges placed on the H atoms. The difference between the two models is the location of the negative point charge. The TIP4P model has one negative charge, which is located at a point 0.15 Å off the oxygen and along the bisector of the HOH bond angle. In contrast, the TIP5P model has two negative-charge sites which are 0.70 Å away from the oxygen and are in the tetrahedral direction of two lone pairs.

For both models, the pairwise potential function is composed of two terms, a 12-6 Lennard-Jones potential term which describes the interaction between oxygens, and a Coulomb potential term as interaction between charged sites. In

a)Electronic mail: htanakaa@cc.okayama-u.ac.jp

the case of the TIP4P potential function, the Lennard-Jones energy parameter, the Lennard-Jones size parameter, and the magnitude of positive charge are $\varepsilon_o = 0.1550$ kcal mol^{-1}, $\sigma_o = 3.15365$ Å, and $q_H = 0.520e$, respectively. The corresponding three parameters of the TIP5P potential function are $\varepsilon_o = 0.16$ kcal mol^{-1}, $\sigma_o = 3.12$ Å, and $q_H = 0.241e$. When the intermolecular distance r is over 15 Å, a common switching function is applied to the two models to smoothly shift the pairwise potential function to zero at $r = 17$ Å. This treatment of the long range force is similar to the original paper for the TIP5P potential.[12]

Twenty configurations are generated for proton-disordered hexagonal ice. The orientations of individual water molecules are so assinged as to satisfy the Bernal-Fowler rule with a vanishing value of the dipole moment but otherwise random. The potential energy of each system is minimized by applying the steepest descent method prior to the normal mode analysis, the calculation of radial distribution functions, etc. The structure thus obtained corresponds to that at temperature 0 K.

B. Free energy calculation of liquid water

To calculate the free energy of liquid water, we employ the thermodynamic integration method.[15,16] This method has been successfully applied to free energy calculations for atomic[15,17] and orientationally disordered molecular system.[18] With this method, computer simulations can be performed for any system with the potential energy function of the form

$$U(\lambda) = U_0 + \lambda^k (U_1 - U_0), \tag{1}$$

where U_0 is the potential energy function of a simple reference system whose free energy can be evaluated analytically, and U_1 is the potential energy function of the system to be studied. In Eq. (1), k is generally a positive integer and λ is a coupling parameter for which $\lambda = 0$ corresponds to the reference system, and $\lambda = 1$ corresponds to the model system to be studied. In the simulation, $\langle \partial U(\lambda)/\partial\lambda \rangle_{N,V,T,\lambda}$ are calculated for various λ values from $\lambda = 0$ to $\lambda = 1$, which give the Helmholtz free energy difference of the reference and the model system, as

$$\Delta A = \int_0^1 \left\langle \frac{\partial U(\lambda)}{\partial \lambda} \right\rangle_{N,V,T,\lambda} d\lambda, \tag{2}$$

where $\langle \rangle_{N,V,T,\lambda}$ denotes the ensemble average taken under fixed number of molecules N, volume V, temperature T, and the coupling parameter λ.

For liquid water, the ideal gas of rigid nonlinear molecules is generally chosen as the reference system. Thus in Eq. (1), $U_0 = 0$. In addition, $k = 4$ is chosen here for calculating the free energy of liquid water. Note that, for the ideal gas, the Helmholtz free energy can be written in an analytical form,

$$A^{id} = N k_B T \left\{ \ln \rho - 1 + \ln \Lambda^3 - \ln \left[\frac{\pi^{1/2}}{\sigma} \left(\frac{8\pi^2 I_A k_B T}{h^2} \right)^{1/2} \times \left(\frac{8\pi^2 I_B k_B T}{h^2} \right)^{1/2} \left(\frac{8\pi^2 I_C k_B T}{h^2} \right)^{1/2} \right] \right\}, \tag{3}$$

where k_B is the Boltzmann constant, ρ is the density of liquid water, Λ is the thermal wave length, I_A, I_B, and I_C are the principal moments of inertia of a water molecule, and the symmetry number σ is 2. The free energy difference from the ideal gas reference, namely, the excess Helmholtz free energy, can then be calculated from Eq. (2). Once the Helmholtz free energy is known, the Gibbs free energy can be calculated via $G = A + PV$, where V is the equilibrium volume, obtained from the N-P-T simulation in advance.

C. Free energy calculation of ice Ih

We calculate the free energy of ice Ih using a different method developed, instead of the conventional thermodynamic integration method. The Helmholtz free energy of ice Ih, which is function of the temperature T and the volume V, can be expressed as

$$A(T,V) = U_q(V) + F_h(T,V) + F_a(T,V) - TS_c, \tag{4}$$

where $U_q(V)$, $F_h(T,V)$, and $F_a(T,V)$ are the potential energy of the system in equilibrium position at temperature 0 K, the harmonic vibrational free energy, and anharmonic vibrational free energy, respectively. S_c stands for the configurational entropy and is given by $k_B N \ln(3/2)$ for N molecule proton-disordered system.

The harmonic vibrational free energy is given by

$$F_h(T,V) = k_B T \sum_i \ln(\hbar \omega_i / k_B T), \tag{5}$$

where $\hbar$ and ω_i are the Planck constant divided by 2π and the ith mode angular frequency. These frequencies are obtained by normal mode analysis, which is performed by diagonalizing the mass weighted force constant matrix.

The anharmonic vibrational free energy can be determined from the relation

$$\frac{F_a(T_0,V)}{T_0} = -\int_0^{T_0} \frac{U_a}{T^2} dT, \tag{6}$$

where U_a is the anharmonic vibrational energy. U_a is given by

$$U_a = U - U_q - U_h, \tag{7}$$

where U is the potential energy calculated from the molecular dynamics (MD) simulation in the N-T-V ensemble and U_h is the harmonic vibrational energy which is given by $3Nk_BT$.

The Gibbs free energy shows a minimum against volume variation when the temperature and pressure are fixed. Based on this thermodynamics principle, we undertook the free energy minimization with respect to the volume to determine the equilibrium Gibbs free energy at designated temperature and pressure. Using this approach, we are able to obtain the equilibrium Gibbs free energy and volume of ice Ih simultaneously.

D. Computational details

In the MD simulation of proton-disordered hexagonal ice, we used 576 molecules in a rectangular box with the periodic boundary conditions. The MD time step is equal to

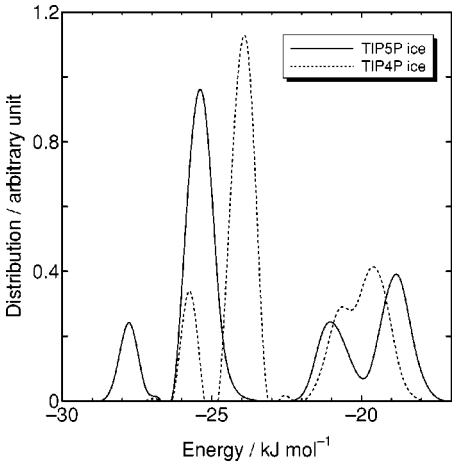

FIG. 1. Pair interaction energy distributions for TIP5P ice (solid line) and TIP4P ice (dotted line).

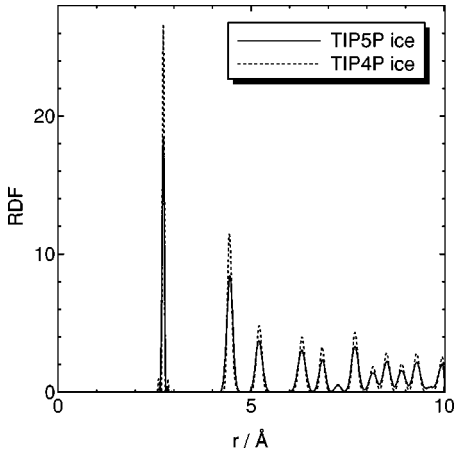

FIG. 2. Radial distribution functions for TIP5P ice (solid line) and TIP4P ice (dotted line).

0.4 fs. We spent 100 000 steps for each N-T-V ensemble simulation. The first 50 000 steps were thrown away and the next 50 000 steps were used for the ensemble averaging.

In the MD simulation of liquid water, we used 512 molecules in a cubic box with the periodic boundary conditions. To determine the equilibrium volume, we carried out N-P-T ensemble simulation with 15 000 000 time steps. The first 5 000 000 steps were discarded and the next 10 000 000 steps were used to obtain the equilibrium volume. N-T-V-λ ensemble simulation was performed for 3 500 000 time steps. After an initial equilibration period of the 500 000 steps, we accumulate the desired quantities for the rest of 3 000 000 steps. As pointed out previously,[19] for proton-disordered hexagonal ice, the calculated melting point is extremely sensitive to the accuracy of free energy calcualtion. Here, we used much longer simulation steps particularly for the liquid free energy calculation so that we can reduce the effects of statistical errors to the determination of the melting temperature.

Our simulation covers the temperature range from 0 K to 300 K and the pressure range from 0.1 MPa to 200 MPa.

III. RESULTS AND ANALYSIS

The pair potential energy distributions at temperature 0 K for the TIP4P ice and the TIP5P ice are shown in Fig. 1. There are four peaks for both the TIP4P ice and the TIP5P ice. The four peaks for the TIP5P ice are all lower and broader than the corresponding ones for the TIP4P ice. Among them, two peaks appear around the energy value $-20\ \mathrm{kJ\,mol^{-1}}$ for both ices. But other two peaks for the TIP5P ice appear at lower energy region by about $2\ \mathrm{kJ\,mol^{-1}}$ than the ones for the TIP4P ice.

To examine the structural differences between the TIP4P ice and the TIP5P ice at 0 K, we calculate the radial distribution functions (RDF) as well as the dihedral angle distributions, shown in Figs. 2 and 3, respectively. The dihedral angle is defined as the angle made by the O—H covalent bonds of a hydrogen-bonded pair when viewed in the direction of the hydrogen-bond axis. The peak heights of the RDF for the TIP5P ice are all lower than the corresponding ones for the TIP4P ice. In particular, the first peaks which describe the hydrogen-bonded pair are different from each other. The broader first peak for the TIP5P ice is consistent with the wider pair potential energy distributions shown in Fig. 1. The dihedral angles in the ice Ih range from 0 to π, with an interval of $\pi/3$. Thus, there are four distinct angles. One can see from Fig. 3 that there are four hydrogen-bond patterns in proton-disordered hexagonal ice, again, consistent with the fact that the pair potential energy distributions show four distinct peaks in Fig. 1. The two peaks at the dihedral-angle value 0 and $\pi/3$ for the TIP5P ice are clearly higher than those for the TIP4P ice. Hence there exists stronger restriction in the rotational motion in the TIP5P ice than in the TIP4P ice. This rotation restriction stems from the geometric difference between the two water models, that is, three charge sites versus four charge sites. The four charge-site model gives rise to a higher energy barrier and thus results in more hindered rotation and a lower potential energy at finite temperature.

The results of normal mode analysis for the TIP4P ice and the TIP5P ice are shown in Fig. 4. The density of state (DOS) for intermolecular vibrational motions is fully split into two parts, due to translation-dominant and rotation-

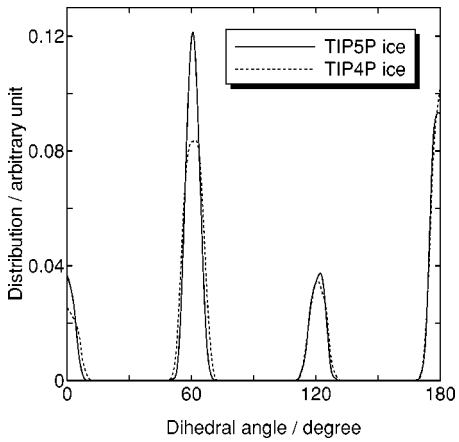

FIG. 3. Dihedral angle distributions for individual water molecules for TIP5P ice (solid line) and TIP4P ice (dotted line).

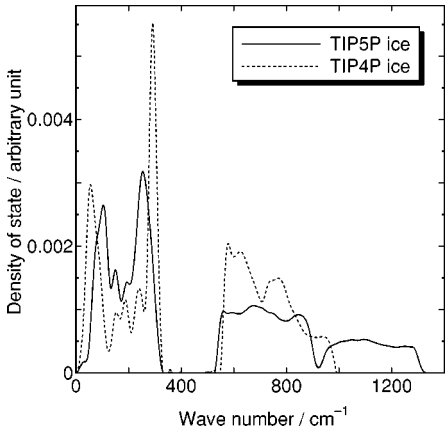

FIG. 4. Densities of state for intermolecular vibrational motions for TIP5P ice (solid line) and TIP4P ice (dotted line).

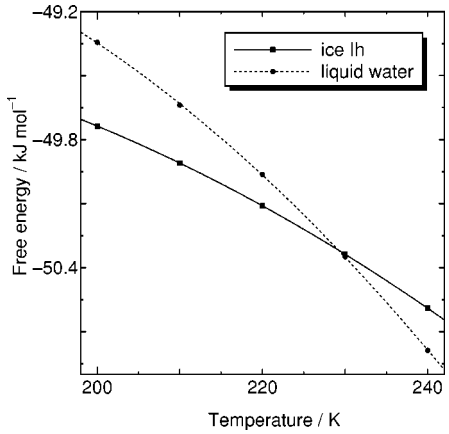

FIG. 6. Temperature dependence of the Gibbs free energies at atmospheric pressure for TIP4P ice (solid line) and liquid water (dotted line).

dominant motions as has been shown.[20,21] The low frequency modes correspond to the translational molecular motions and the high frequency modes correspond to the rotational molecular motions. There are two sharp peaks for the translational molecular motions. The lower peak is associated with the bending motion of three hydrogen-bonded molecules and the higher one is associated with a stretching motion of a hydrogen-bonded pair. For the TIP5P ice, the former appears around 100 cm^{-1}, and the latter appears around 250 cm^{-1}. The DOS for the TIP5P ice spreads out in the high frequency region, compared to the DOS spectrum for the TIP4P ice. This feature has also been seen in the ST2 model, another popular model with four charge sites similar to the TIP5P model. The DOS of the TIP4P ice, however, is closer to that of realistic ice Ih.[22] High frequency region of the DOS for the TIP5P ice is hardly responsible to the melting, because the mode displacement is decreasing as the mode frequency is higher.

In Figs. 5 and 6, we show the Gibbs free energy curves for both liquid and ice Ih phases of TIP5P water and those for TIP4P water, respectively. It can be seen that the slopes of both free energy curves are negative in the temperature range considered, which means the entropies S are always positive as $S=-(\partial G/\partial T)_P$. The melting temperature can be determined from the point at which the two free energy curves intersect. The melting temperatures of the TIP4P ice and the TIP5P ice at the ambient pressure are 229 ± 9 K and 268 ± 6 K, respectively. Compared with the experimental value (273 K), that of the TIP4P ice is 50 K lower, while the melting temperature of the TIP5P ice is nearly the same as experimental value. The changes of the thermodynamic properties at the melting point are listed in Table I. The TIP5P ice gives better agreement with the experimental values[23] than the TIP4P ice except for the volume change. The pressure dependences of the melting temperature for both the TIP4P and the TIP5P ices are shown in Fig. 7. The lines in Fig. 7 represent the ice-liquid phase boundaries, which show negative slopes as the experimental phase boundary.

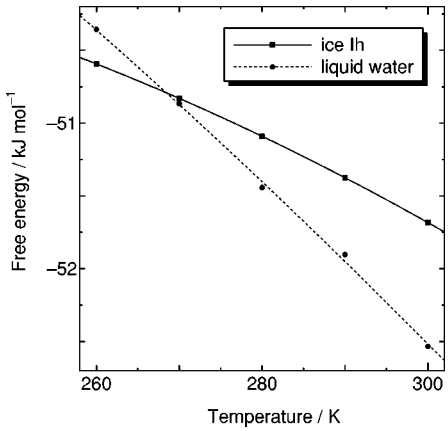

FIG. 5. Temperature dependence of the Gibbs free energies at atmospheric pressure for TIP5P ice (solid line) and liquid water (dotted line).

We display the thermal expansivity curves of the TIP4P ice, the TIP5P ice, and the ST2 ice in Fig. 8. The thermal expansivity of the TIP4P ice is negative up to about 60 K, but that of the TIP5P ice is always positive in the low temperature region. For the ST2 ice the thermal expansivity is only slightly negative in the low temperature region (which is hardly seen from Fig. 8). The negative thermal expansivity is caused largely by low frequency modes, each of which has a negative mode Grüneisen parameter. The Grüneisen parameter of the ith mode, γ_i is given by

$$\gamma_i=-(\partial \ln \omega_i/\partial \ln V), \tag{8}$$

and the Grüneisen parameter of the system, γ is given by

$$\gamma=\sum_i \gamma_i C_i \Big/ \sum_i C_i, \tag{9}$$

TABLE I. Variation of thermodynamic properties caused by melting at 0.1 MPa.

	TIP4P	TIP5P	Exp.
ΔV (cm^3 mol^{-1})	−1.394	−0.651	−1.621
ΔH (kJ mol^{-1})	3.384	5.971	6.014
ΔS (J K^{-1} mol^{-1})	14.78	22.25	22.01

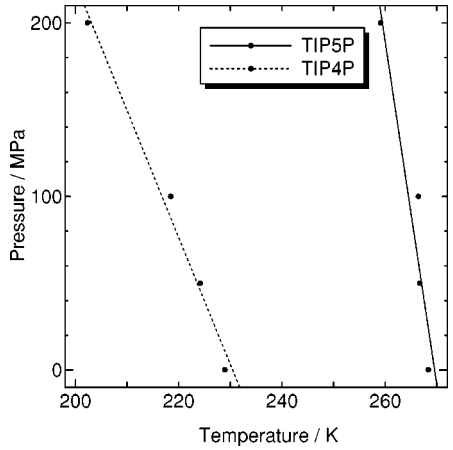

FIG. 7. Ice-liquid phase boundaries of TIP5P ice (solid line) and TIP4P ice (dotted line).

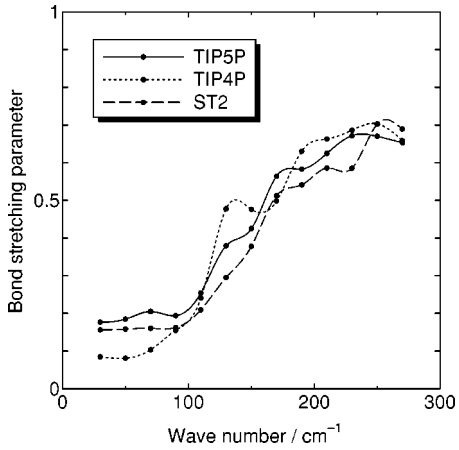

FIG. 9. Bond stretching parameters of TIP5P ice (solid line), TIP4P ice (dotted line), and ST2 ice (dashed line).

where C_i is the heat capacity of the ith mode. The relation between the thermal expansivity α and γ is

$$\alpha = \gamma C_v \kappa_T / 3V, \tag{10}$$

where C_v is the heat capacity at constant volume of the system and κ_T is the isothermal compressibility. In Eq. (9), C_v, κ_T, and V are always positive, and hence negative γ always gives a negative α. For the TIP4P ice, the vibrational modes with frequency less than 100 cm^{-1} all have a negative γ_i, which are correspondent to about 15% of all the normal modes. For the ST2 ice, the low-frequency vibrational modes also have negative γ_i, but the number of such modes is about 50% less than that for the TIP4P ice. On the other hand, no vibrational mode has negative γ_i for the TIP5P ice. As a result, its thermal expansivity cannot be negative. The contribution to γ from those low-frequency modes with negative γ_i should be large enough to give rise to negative thermal expansivity at the low temperature. To examine the character of the low-frequency modes, we calculate the bond-stretching parameter S_k,[24] which is defined as

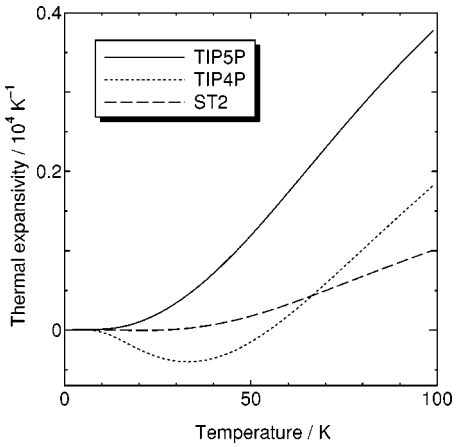

FIG. 8. Thermal expansivities of TIP5P ice (solid line), TIP4P ice (dotted line), and ST2 ice (dashed line) at atmospheric pressure as a function of temperature.

$$S_k = \left[\frac{\Sigma_{i,j} |(\mathbf{u}_i^k - \mathbf{u}_j^k) \cdot \mathbf{n}_{ij}|^2}{\Sigma_{i,j} |(\mathbf{u}_i^k - \mathbf{u}_j^k)|^2} \right]^{1/2}, \tag{11}$$

where $\mathbf{u}_i^k$ is the displacement vector of the ith molecule associated with the kth mode, and $\mathbf{n}_{ij}$ is the unit vector from the ith molecule to the jth molecule for a directly hydrogen-bonded pair. If the value of S_k is close to unity, the kth mode is mostly bond-stretching. That the value is close to zero indicates the bond-bending modes. In Fig. 9, we plot the bond-stretching parameters of the TIP4P ice, the TIP5P ice, and the ST2 ice. For all three model ices, the parameter value is close to zero at the low frequency region below 70 cm^{-1}, that is, the modes are mainly composed of the bending motion. The bending motion is more significant in the TIP4P ice than in the ST2 ice and the TIP5P ice. When the low frequency modes no longer give rise to negative γ_i as decreasing the bending motion, the negative thermal expansivity disappears.

IV. CONCLUSION

From the calculated free energies of the proton disordered hexagonal ice and the liquid water, we obtain the melting points of the TIP4P ice and the TIP5P ice at atmospheric pressure to be $T_m = 229 \pm 9$ K and $T_m = 268 \pm 6$ K, respectively. The TIP5P model greatly improves the melting temperature compared to the TIP4P model. We calculate changes of thermodynamic properties at the ice-liquid phase transition at atmospheric pressure. We find that ΔV of the TIP4P model is closer to the experimental value than that of the TIP5P model. However, for the ΔH and ΔS, the TIP5P model gives better agreement with the experiment than the TIP4P model. Both models give the ice-liquid phase boundaries with negative slopes in accordance with the real water. We conclude that the TIP5P model can be specifically useful for the computer simulation dealing with liquid water at atmospheric pressure.

The TIP5P model cannot reproduce the negative thermal expansivity in the low temperature region, as opposed to the TIP4P model. The negative thermal expansivity arises from the low frequency vibrational modes with negative Grüneisen parameter. However, these modes are not observed in

the low frequency region for the TIP5P ice. We find that the modes with the negative Grüneisen parameter are associated with the bending motions of tetrahedrally hydrogen bonded molecules. Based on the calculated bond-stretching parameter, the low frequency modes of the TIP4P ice show much stronger bending motions than the TIP5P ice. This difference in the mode character at low frequency region provides an explanation to the vanishing negative thermal expansivity for the TIP5P ice.

ACKNOWLEDGMENTS

This work was supported by grant-in-aid from JSPS and Ministry of Education in Japan, by Okayama Foundation for Science and Technology, by NAREGI nanoscience project, and grants by NSF and DoE. The authors are grateful to Professor K. Koga for stimulating discussion.

[1] H. J. C. Berendsen, J. P. M. Postma, W. F. van Gunsteren, and J. Hermans, in *Intermolecular Forces*, edited by B. Pullman (Reidel, Dordrecht,1981), p. 331.
[2] H. J. C. Berendsen, J. R. Grigera, and T. P. Straatsma, J. Phys. Chem. **91**, 6269 (1987).
[3] W. L. Jorgensen, J. Chandrasekhar, J. D. Madura, R. W. Impey, and M. L. Klein, J. Chem. Phys. **79**, 926 (1983).
[4] W. L. Jorgensen and J. D. Madura, Mol. Phys. **56**, 1381 (1985).
[5] S. R. Billeter, P. M. King, and W. F. van Gunsteren, J. Chem. Phys. **100**, 6692 (1994).
[6] P. H. Poole, F. Sciortino, U. Essman, and H. E. Stanley, Nature (London) **360**, 324 (1992); Phys. Rev. E **48**, 3799 (1993); **55**, 727 (1997).
[7] W. L. Jorgensen and C. Jenson, J. Comput. Chem. **19**, 1179 (1998).
[8] F. H. Stillinger and A. Rahman, J. Chem. Phys. **60**, 1545 (1974).
[9] F. Sciortino and S. Sastry, J. Chem. Phys. **100**, 3881 (1994).
[10] I. M. Svishchev, P. G. Kusalik, J. Wang, and R. J. Boyd, J. Chem. Phys. **105**, 4742 (1996).
[11] A. Wallqvist and B. J. Berne, J. Phys. Chem. **97**, 13841 (1993).
[12] M. W. Mahoney and W. L. Jorgensen, J. Chem. Phys. **112**, 8910 (2000).
[13] G. Dantl, Z. Phys. **166**, 115 (1962).
[14] H. Tanaka, J. Chem. Phys. **108**, 4887 (1998).
[15] D. Frenkel and A. J. C. Ladd, J. Chem. Phys. **81**, 3188 (1984).
[16] D. Frenkel and B. Smit, *Understanding Molecular Simulation* (Academic, San Diego, 1996).
[17] B. B. Laird and A. D. J. Haymet, Mol. Phys. **75**, 71 (1992).
[18] E. J. Meijer, D. Frendel, R. A. LeSar, and A. J. C. Ladd, J. Chem. Phys. **92**, 7570 (1990).
[19] G. T. Gao, X. C. Zeng, and H. Tanaka, J. Chem. Phys. **112**, 8534 (2000).
[20] J. S. Tse, J. Chem. Phys. **96**, 5482 (1992).
[21] I. Ohmine and H. Tanaka, Chem. Rev. (Washington, D.C.) **93**, 2545 (1993).
[22] J.-C. Li, J. Chem. Phys. **105**, 6733 (1996).
[23] D. Eisenberg and W. J. Kauzmann, *The Structures and Properties of Water* (Clarendon, London, 1969).
[24] J. Fabian and P. B. Allen, Phys. Rev. Lett. **79**, 1885 (1997).